ARTICLE

Carbazole modification of Ruthenium Bipyridine–dicarboxylate Oxygen Evolution Molecular Catalyst

Received 00th January 20xx,
Accepted 00th January 20xx

DOI: 10.1039/x0xx00000x

Hiroki Otsuka,[a] Atsushi Kobayashi,*[,a] Masaki Yoshida,[a] and Masako Kato[a,b]

We newly synthesized oxygen-evolving molecular Ru(II) catalysts with one or two carbazole moieties on the axial pyridyl ligands, namely [Ru(bda)(cbz-py)(py)] and [Ru(bda)(cbz-py)$_2$] [**C1** and **C2**; bdaH$_2$ = 2, 2′-bipyridyl-6, 6′-dicarboxylic acid; py = pyridine, cbz-py = 9-(pyridin-4-yl)-9*H*-carbazole] to investigate the effect of cbz modification on the photophysical and catalytic properties of the well-known molecular catalyst [Ru(bda)(py)$_2$] (**C0**). The initial oxygen-evolving catalytic activities of **C1** and **C2** were higher than that of **C0** in both a chemical reaction driven by the strong oxidant $(NH_4)_2[Ce(NO_3)_6]$ (CAN = Ceric ammonium nitrate) and a photochemical oxidation using a $[Ru(bpy)_3]^{2+}$ (bpy = 2,2′-bipyridine) photosensitizer with $Na_2S_2O_8$ as the sacrificial oxidant. The higher activities were ascribed to the electron-withdrawing cbz groups, which promoted the radical coupling reaction to form a Ru^{IV}–O–O–Ru^{IV} species. A unique oxygen-evolution rate change behaviour was observed for both **C1** and **C2** in the presence of a large excess of CAN, suggesting competitive oxidation of the cbz moiety during the chemical oxygen evolution reaction. This work suggests that cbz modification of an oxygen evolution molecular catalyst is a promising approach to integrate the hole accumulator near the oxygen evolution catalytic centre.

Introduction

Visible-light water-photolysis reaction is a promising reaction for converting solar energy into hydrogen, a clean chemical energy resource. In this reaction, water oxidation, especially the oxygen evolution reaction (OER; $2H_2O \rightarrow O_2 + 4H^+ + 4e^-$), is a half-reaction that provides protons and electrons for the hydrogen evolution reaction. However, this reaction is considered to be one of the bottlenecks in water splitting reactions because it requires multi-electron and multi-proton transfer. [1] The development of high-performance water oxidation catalysts (WOCs) for photoreaction systems using molecular materials [2] together with efficient combination methods with photoreaction systems are being explored to drive the highly efficient OER. The direct connection of WOCs and photosensitizers (PS) as supramolecular homogeneous catalysts [3] or photoelectrodes [3a, 4] is a promising method for promoting photoinduced through-bond electron transfer. Further development to introduce redox mediators to accumulate holes near WOC have been recently reported. [5]

In this context, carbazole (cbz) derivatives with high electron mobility and positive redox potentials [6] are promising candidates as hole mediators in OER reaction systems. One example is the application of Cu(I) PS with cbz as an electron donor moiety for an OER photoanode [7] and electrochemical OER anodes with polycarbazole as hole-transporters. [8a] In particular, polycarbazole systems are expected to affectively couple with WOCs and PSs. Several studies have suggested that the OER catalytic activity was improved by modifying the polycarbazole-functionalized WOCs on the electrode surface. [8] However, to the best of our knowledge, the effect of cbz modification on the OER catalytic activity of molecular WOC homogeneous systems have been hardly elucidated so far.

In this study, to elucidate the effect of cbz functionalization on the OER, we newly synthesized two complexes, [Ru(bda)(cbz-py)(py)] and [Ru(bda)(cbz-py)$_2$] (Fig. 1, **C1** and **C2**), comprising a Ru-bda (bdaH$_2$ = 2, 2'-bipyridyl-6, 6'-dicarboxylic acid) complex backbone modified with one or two cbz-py moieties, respectively. The redox mediating cbz group attached on the axial py ligand may adversely affect the catalysis through

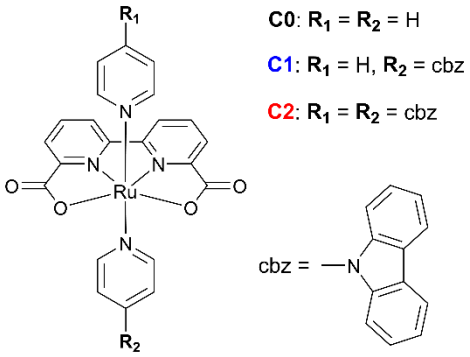

Fig. 1. Molecular structure of the complexes **C0**, **C1,** and **C2**.

[a] *Department of Chemistry, Faculty of Science, Hokkaido University, North-10 West-8, Kita-ku, Sapporo 060-0810, Japan. Email: akoba@sci/hokudai.ac.jp (A.K.)*
[b] *Department of Applied Chemistry for Environment, School of Biological and Environmental Sciences, Kwansei Gakuin University, 2-1 Gakuen, Sanda, Hyogo 669-1337, Japan.*

† Footnotes relating to the title and/or authors should appear here.
Electronic Supplementary Information (ESI) available: [details of any supplementary information available should be included here].

See DOI: 10.1039/x0xx00000x

electrostatic interactions on WOCs with bimolecular O-O coupling process, including Ru-bda complexes, which is one of the most popular molecular WOC in photo- and/or electrochemical OERs, owing to its high catalytic activity, stability, and ligand tunability.[9] We observed that the introduced cbz group(s) acted as the electron-withdrawing group(s) to improve the OER activity during the early stage of the reaction. The effect of the oxidation process of the cbz group on chemical and photochemical oxygen evolution catalysis was also investigated in detail.

Results and discussion

Photophysical and electrochemical properties

The photophysical and electrochemical properties of **C1** and **C2** were investigated to elucidate the effect of cbz functionalization on the molecular catalyst **C0**. The UV-vis absorption spectra in dichloromethane/2,2,2-trifluoromethanol (TFE) are shown in Fig. 2. The cbz-comprising complexes **C1** and **C2** presented similar spectra to those of **C0**, but with new sharp absorption peaks at 286 nm and 334 nm. Similar absorption peaks, at near-identical positions, were observed for the cbz-py ligand. Thus, these two absorption bands were assigned to the intra-ligand transition (^{1}LC) of the cbz-py ligand. In the wavelength range above 350 nm, two contrasting trends were observed: The band at ~370 nm was more strongly observed in **C1** and **C2** than **in C0**, while the absorbances of the bands at 475 and 531 nm were near-identical to those of **C0**. In the case of **C0**, the absorption band at 370 nm was assigned as the ^{1}MLCT transition to the pyridine ligand, while those at 475 and 531 nm are other ^{1}MLCT transitions to the bda ligand.[9, 10] The molecular structures of **C1** and **C2** are near-identical to that of **C0**, except for the cbz group(s), and thus, the same MLCT transitions to py or the bda ligands were also observed for these cbz-functionalized complexes. These assignments are validated because the absorbances of the lower-energy MLCT transitions to the bda ligands are near-identical in these three complexes. A higher absorbance of the MLCT transition to the py ligand, with a slight red shift in **C1** and **C2** compared to that in **C0,** was observed. This was ascribed to the π-extension of the py ligand by cbz functionalization, which leads to an increase in the transition dipole moment. In the mixture containing water, these absorption bands were shifted to shorter wavelengths by ~40 nm (Fig. S1). This solvatochromic behaviour is further evidence of the CT nature of these absorption bands.

Differential pulse voltammetry (DPV) was performed to evaluate the effect of the introduced cbz group on the redox properties. As shown in Fig. 3, two oxidation peaks attributed to the redox couples, $Ru^{III/II}$ and $Ru^{IV/III}$, were observed in both complexes, as reported for **C0** (Table 1). A peak assigned to $Ru^{III/II}$ was observed at 0.8–0.9 V vs NHE, similar to that reported for **C0** in acetonitrile. This suggests that these complexes mainly exist as a structure in which the acetonitrile solvent is coordinated to the Ru centre under this solvent condition.[10a, 11] The redox potential of $Ru^{III/II}$ was slightly shifted to positive in the order **C0** (0.85 V vs NHE) < **C1** (0.87 V) < **C2** (0.90 V). These results were attributed to the substituent effect of the cbz group introduced in **C1** and **C2**, as reported for the electron-withdrawing-group-functionalized [Ru(bda)(py)$_2$] series.[10] This is supported by the fact that [Ru(bda)(4-bromopyridine)$_2$] (**C0-Br**) modified with a Br group, which comprises a more electron-withdrawing substituent, showed a more positive $Ru^{III/II}$ redox potential (0.92 V, Fig. S2) than did the others. On the other hand, the oxidation peaks of $Ru^{IV/III}$, observed on the more positive side of the redox potential, were all similar at 1.13–1.14 V (Table 1). This is consistent with a previous report that the substituent effect is negligible in the redox potential of $Ru^{IV/III}$.[10a-c] In addition to the redox couples of the Ru centre, **C1** and **C2** showed marked oxidation peaks in the more positive potential region (1.4–1.5 V vs NHE), in which **C0** did not present any peaks.

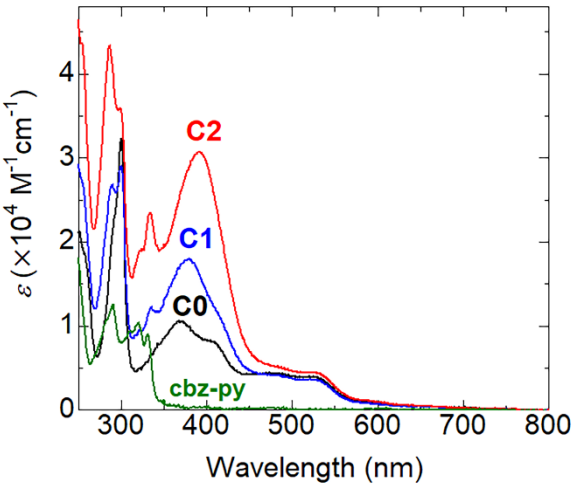

Fig. 2. UV-vis absorption spectra of the **C0** (black), **C1** (blue), **C2** (red) complexes and cbz-py (green) ligand (10 μM, dichloromethane/TFE, v/v = 9/1).

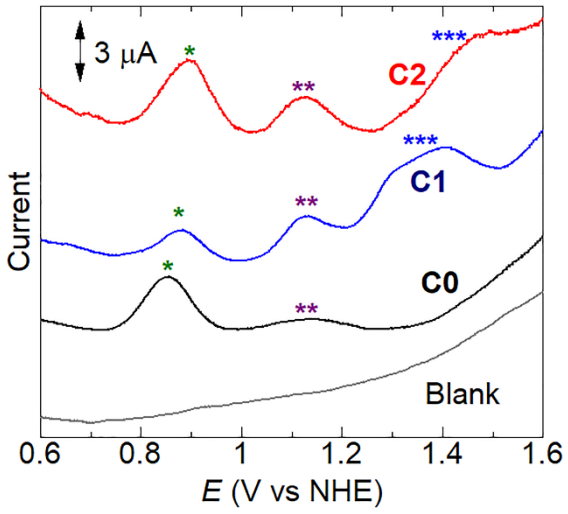

Fig. 3. DPV curves of the complexes **C0** (black), **C1** (blue), and **C2** (red) in pH = 1.0 $HClO_4$ aq./TFE/acetonitrile (v/v/v = 3/2/1) containing 0.1 M $NaClO_4$; scan rate = 10 mVs^{-1}. Single (*), double (**), and triple asterisks (***) denote a redox couple of $Ru^{III/II}$, $Ru^{IV/III}$, and a cascade of $Ru^{V/IV}$ and (cbz^{ox}/cbz), respectively.

Table 1. Redox potentials of **C0**, **C1**, and **C2** estimated by DPV measurement.

Complex	$E(Ru^{III/II})$ ($V_{vs\ NHE}$)	$E(Ru^{IV/III})$ ($V_{vs\ NHE}$)	$E(cbz^{ox}/cbz)^a$ ($V_{vs\ NHE}$)
C0	0.85	1.14	n.d.
C1	0.87	1.13	1.41
C2	0.90	1.13	1.48

[a] Irreversible in aqueous solution.

Because the cbz-py ligand also exhibited a similar oxidation wave [Fig. S3(a)], the oxidation wave at ~1.4 V should include the oxidation current of the cbz groups in **C1** and **C2**. Although similar redox behaviour was observed in the CV of the water-containing mixtures [Fig. S3(b)], the oxidation waves of the cbz group gradually disappeared by repeating the potential sweep of the CV cycles. In fact, the large cbz oxidation peak of **C2** almost disappeared after only three potential sweep cycles [Fig. S4(b)], while the cbz oxidation current decay of **C1** was significantly slower (~50 cycles) than that of **C2** [Fig. S4(a)]. This difference indicates that the number of cbz groups in one molecule is a crucial factor in the redox behaviour. A similar trend was reported for the electrode bearing Ru-bda complexes connected to the cbz moiety by a long alkoxy chain. [8b] Thus, the rapid current decrease of the cbz oxidation for **C2** in aqueous solvent suggests that an irreversible conversion to an oxidized species would be triggered by the cbz oxidation.

Theoretical calculation

In $[Ru(bda)(py)_2]$-type molecular catalysts, the electron-withdrawing functional group attached on the py ligand plays an important role on both the physical properties and catalytic activities. [10] Our electrochemical measurements for **C1** and **C2** revealed that the shifts of the $Ru^{III/II}$ redox couple of these cbz-functionalized complexes were more positive than that of **C0**, suggesting the electron-withdrawing nature of the cbz moiety. [12] To gain further insight into the effect of the cbz group, density functional theory (DFT) calculations were carried out using Gaussian 09 W. Fig. 4(a) shows the schematic molecular orbital (MO) energy diagrams for **C0**, **C1**, and **C2**, while the energy of each MO is listed in Table S1. In all three complexes, the highest occupied molecular orbital (HOMO) is localised in the t_{2g} orbital of the central Ru(II) ion (Fig. 4(b)), and the orbital energy is stabilized in the order **C0** (-4.8747 eV) > **C1** (-4.9008 eV) > **C2** (-4.9247 eV), depending on the number of cbz moieties. Generally, a stronger π-accepting ligand generates a larger ligand field splitting of the central metal ion, resulting in more stabilized t_{2g} orbitals in the octahedral coordination geometry. Thus, compared to that of **C0**, the stabilized HOMOs of **C1** and **C2** indicate the electron-withdrawing nature of the cbz moiety. This well-agrees with the positive shift of the $Ru^{III/II}$ redox couple, as estimated from the DPV measurements (Fig. 3). Similar stabilisation was also observed for the lowest unoccupied molecular orbital (LUMO) and LUMO+3, wherein the energies of these unoccupied orbitals also decreased with increasing number of cbz groups. Here, the LUMO was stabilized because it comprises both the π* orbital of the bda ligand and d orbital of the Ru(II) centre (Table S1). Because LUMO+3 is localised on

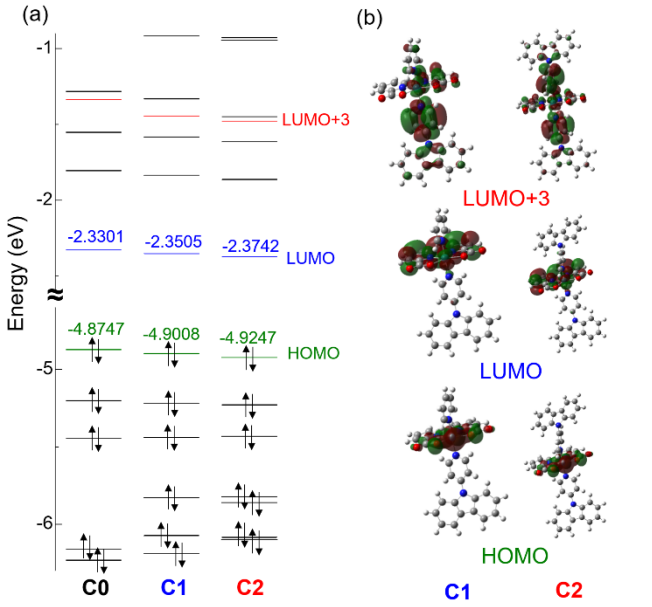

Fig. 4. (a) Schematic MO energy diagram for **C0**, **C1,** and **C2** and (b) MO distributions of HOMO, LUMO, and LUMO+3 of **C1** and **C2**.

the π* orbitals of the py ligand, the stabilized LUMO+3 for **C1** and **C2** over that of **C0** should originate from the electron-withdrawing nature of the cbz group. In addition, as previously discussed, the effect of the cbz moiety on the [Ru(bda)(py)] molecule is similar to that of the Br-functionalized complex (**C0-Br**). Thus, we concluded that the cbz group attached to the py ligand acts as an electron-withdrawing substituent, as suggested by the electrochemical measurements.

We also conducted time-dependent density functional theory (TD-DFT) calculation to gain deeper insight into the photophysical property of **C1** and **C2**. The results are shown in Fig. S5-S8 and Tables S2-S4. The simulated absorption spectra of all three complexes were well agreed to the experimental absorption spectra. The two lowest-energy absorption bands at around 470 and 510 nm with comparable oscillator strength (f = 0.03-0.04) are basically assigned to the MLCT transition from the Ru 4d to π* orbital of bda ligand with slight contribution of the π orbital of py ligand. Two remarkably intense bands (f > 0.1) were appeared in both the simulated spectra of **C1** and **C2** at ~400 nm as the CT transition from the Ru-bda unit to the cbz-py ligand. The orbital of cbz moiety was involved in these transitions (e.g. LUMO+3 of **C1** and **C2**), suggesting that the intense nature should originate from the electron withdrawing nature of cbz moiety, leading to the larger dipole moment of CT transition from Ru-bda to py ligand. On the other hand, the ligand-to-ligand charge transfer (^{1}LLCT) absorption from the π orbital of cbz-py to the bda π* orbital was hardly found in the visible region (λ > 400 nm) of simulated spectra.

Chemical water oxidation

OER with the Ce^{IV} sacrificial oxidant $(NH_4)_2[Ce(NO_3)_6]$ (CAN) was carried out to evaluate the effect of cbz functionalization on the catalytic activity. Fig. 5 shows the results of the OER in the presence of 100 μM **CX** WOC catalyst (**X** = **0**, **1**, **2**) and 120 mM

CAN at room temperature. The estimated turn-over frequency for the initial 30 s of reaction (TOF_i) and maximum TOF (TOF_{max}) are listed in Table 2. All three complexes catalytically evolved O_2, whereas no O_2 evolved in the absence of a WOC. The amounts after 2 min of reaction almost reached a value (150 μmol) corresponding to the complete consumption of CAN when the following reaction occurred:

$2H_2O + 4Ce^{4+} \rightarrow O_2 + 4Ce^{3+} + 4H^+$ (1)

The OER activity (TOF_i and TOF_{max}) of **C2** was higher than those of **C1** and **C0**. This occurs because the electron-withdrawing cbz moieties in **C2** enhance the catalytic activity by destabilizing the $[Ru^V{=}O]^+$ species, thereby leading to the formation of radical couplings (Ru^{IV}–O–O–Ru^{IV} species) as reported in the literature. [10c] On the other hand, the OER activity of **C1** started to decrease after ~45 s, suggesting the presence of deactivation processes. To obtain more detailed information on the reaction mechanism, the catalyst concentration ([Cat.]) dependence of the OER was next investigated [Fig. 6(a-c)]. The OER rate (mM s^{-1}) of all the three complexes decreased with decreasing [Cat.]. Moreover, the linear proportional correlation between the OER rate and square of the catalyst concentration ($[Cat.]^2$) (Fig. S9), suggests that the OER proceeds as a second-order reaction. These results are in good agreement with the proposed reaction mechanism for the Ru-bda catalyst via the Ru^{IV}–O–O–Ru^{IV} species [9, 10] and previous reports on related kinetic analysis. [10a, 13] The O_2 evolved for **C0** and **C1** under [Cat.] = 25 μM conditions approximated 70 μmol after 25 min of reaction. On the other hand, **C2** evolved ~140 μmol O_2 after 12 min reaction, because of the almost complete consumption of CAN as the one-electron oxidant. These results indicate the superior performance of **C2** even at low CAN concentrations. Notably, remarkable changes in the OER rate before the complete consumption of CAN were observed for **C1** and **C2** under low [Cat.] conditions. In particular, at 25 μM for **C2** and below 50 μM for **C1**, the OER rate decreased once within the initial 3 min reaction and then increased again [Fig. 6(b) and 6(c) for **C1** and **C2**, respectively]. This unique behaviour was not observed for **C0**, indicating that the oxidation reaction of the cbz moieties in **C1** and **C2** are key to this unique behaviour. To examine the effect of cbz oxidation, we next investigated the OER of **C0** in the presence of two equivalents of unsubstituted carbazole [cbz-H, Fig. 6(a)]. Only a small amount of oxygen (~5.5 μmol) was produced in the initial 2 min of reaction, after which the OER was paused for 5 min. Subsequently, the OER restarted to generate O_2 (~130 μmol). The oxidation potential of cbz (1.4–1.5 V) in the above-mentioned electrochemical measurements was estimated to be more negative than that of the $Ce^{IV/III}$ redox potential of CAN (1.70 V vs NHE). [14] This suggests that both the Ru centre and the cbz-py ligand can be oxidized by the excess amount of CAN, and thus, that the cbz-oxidized species can be involved in the catalytic OER. Because the oxidation of the cbz moieties in **C1** and **C2** is expected to occur more easily in the presence of a large excess of CAN, the CAN concentration dependence was next investigated with [Cat.] = 50 μM (Fig. S10). No significant change in the TOF_{max} of **C0** was observed by decreasing [CAN]; however, the value for **C1** increased at least threefold when [CAN] was decreased from 120 mM to 90 or 60 mM (Table 2). Notably, this unique behaviour, in which the OER rate changed before the complete consumption of CAN, was hardly observed at lower [CAN]. For **C2**, a decrease in the OER rate was observed after approximately 1 min when [CAN] equalled 120 mM but not with lower concentrations. This infers that the large excess of CAN oxidises the cbz group(s) of **C1** and **C2**, leading to a change in the OER mechanism. The dissociated cbz-py ligand and cbz were hardly observed in the mass spectrum of the extract of the reaction solution of 25 μM **C1** by CH_2Cl_2 (Fig. S11), implying the negligible contribution of the cbz-py dissociated species to this OER rate change behaviour.

Table 2. O_2 evolution catalytic activity of each WOC.[a]

Catalyst	[Cat.] (μM)	[CAN] (mM)	TOF_i (s^{-1})[b]	TOF_{max}(s^{-1})
C0	100	120	0.84	5.6
	50	120	0.51	3.2
	25	120	0.46	1.3
	10	120	0.26	1.0
	50	90	0.28	3.7
	50	60	0.25	3.9
C1	100	120	1.7	4.2
	50	120	1.1	1.9
	25	120	1.0	1.0
	10	120	0.43	1.3
	50	90	3.0	7.3
	50	60	4.0	10
C2	100	120	6.0	11
	50	120	5.1	7.5
	25	120	5.5	7.5
	10	120	4.3	7.6
	50	90	4.0	8.4
	50	60	4.2	7.1

[a] pH = 1.0 $HClO_4$ aq./TFE/acetonitrile (v/v/v = 3/2/1). [b] Estimated from the values obtained for the initial 30 s after mixing.

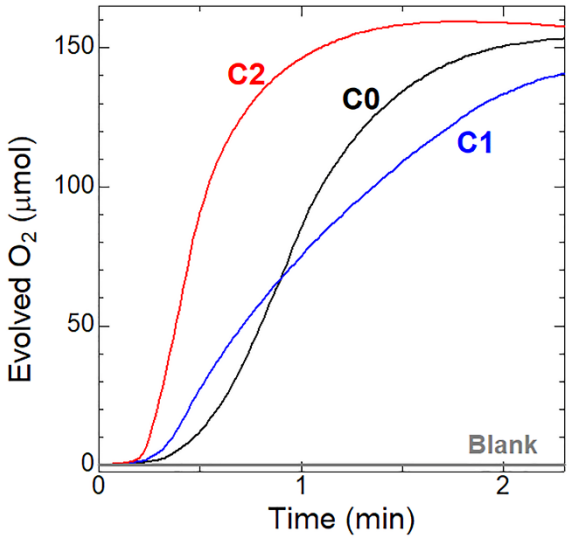

Fig. 5. Chemical OER plots of the complexes **C0** (black), **C1** (blue), and **C2** (red) in pH = 1.0 $HClO_4$ aq./TFE/acetonitrile (v/v/v = 3/2/1), [CAN] = 120 mM, and [Cat.] = 100 μM. Gray line shows the result in the absence of a WOC.

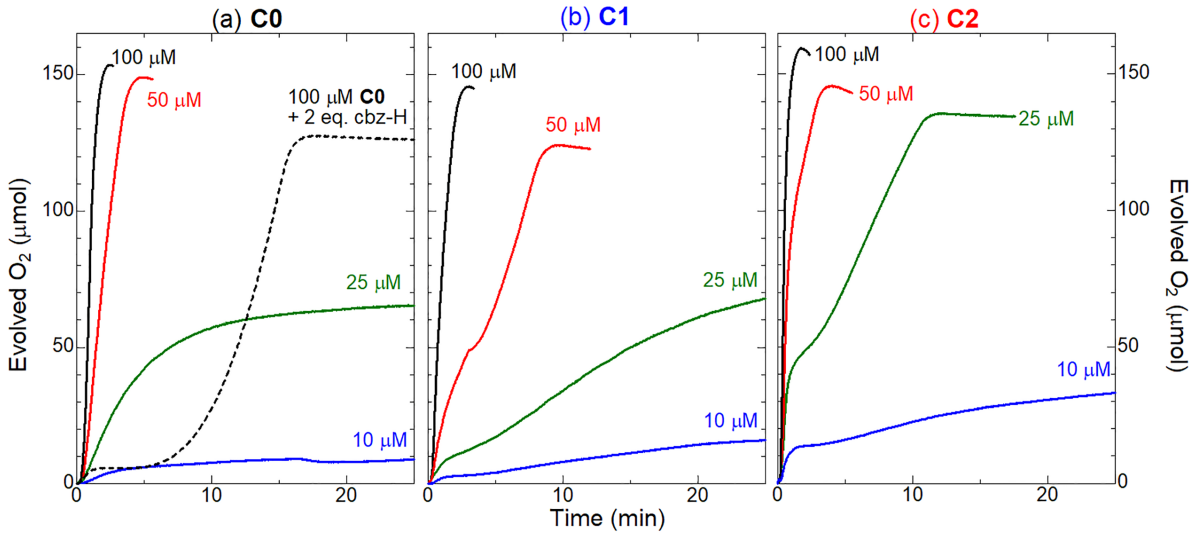

Fig. 6. Catalyst concentration dependence of the chemical OERs of (a) **C0**, (b) **C1,** and (c) **C2**. [CAN] = 120 mM, [Cat.] = 10 μM (blue), 25 μM (green), 50 μM (red), and 100 μM (black) in pH = 1.0 $HClO_4$ aq./TFE/acetonitrile (v/v/v = 3/2/1). Black dotted line in panel (a) shows the chemical OER plots of **C0** in the presence of 2 eq. cbz-H with [Cat.] = 100 μM.

Scheme 1 shows the possible OER mechanism of the cbz-modified catalysts, **C1** and **C2**. The key step for the OER of **C0** is the radical coupling reaction of two Ru^{V}=O species to form the Ru^{IV}–O–O–Ru^{IV} species. For **C1** and **C2,** comprising cbz moieties, in the presence of a large excess of CAN, the oxidation of the cbz group(s) competes with the formation of the Ru^{IV}-O-O-Ru^{IV} species through radical coupling and the subsequent reaction to produce oxygen. Although we did not succeed in characterising the cbz-oxidized species, the formation of nitrocarbazole derivatives from the reaction with CAN has been reported. [15] If such an irreversible oxidation of the cbz moiety occurs, the radical coupling of $[Ru^{V}=O]^{+}$ complexes to form Ru^{IV}–O–O–Ru^{IV} species might be suppressed by steric hindrance and/or electrostatic repulsion between the cbz-oxidized complexes cbz(ox)–$[Ru^{V}=O]^{+}$, resulting in a slower OER. Although the OER activity of the cbz-oxidized species was lower than that of the species without cbz oxidation, these results suggest that the cbz-functionalization of the **C0** molecular catalyst is a promising approach for the integration of the hole-mediator function near the WOC centre.

Photochemical water oxidation

We also conducted photochemical OER in the presence of $[Ru(bpy)_3]^{2+}$ (bpy = 2, 2'-bipyridine) as the PS and $Na_2S_2O_8$ as the sacrificial oxidant. The estimated TOF_{max} and turnover number (TON) for 60 min of reaction are listed in Table 3. As shown in Fig. 7, the photochemical OER activities of **C1** and **C2** in the initial 10 min of reaction were higher than that of **C0**. No O_2 evolution was detected in the absence of $[Ru(bpy)_3]^{2+}$ PS (Fig. S12). The TOF_{max} values were also 1.8 times higher than that of **C0**. These better catalytic activities are ascribed to the contribution of the electron-withdrawing cbz moiety, as discussed above. The photochemical OER rate of **C2** decreased after 10 min of irradiation, and the TON after 1 h of irradiation was less than that of **C0**. However, such a decrease in photochemical OER activity was not observed for **C1**, wherein

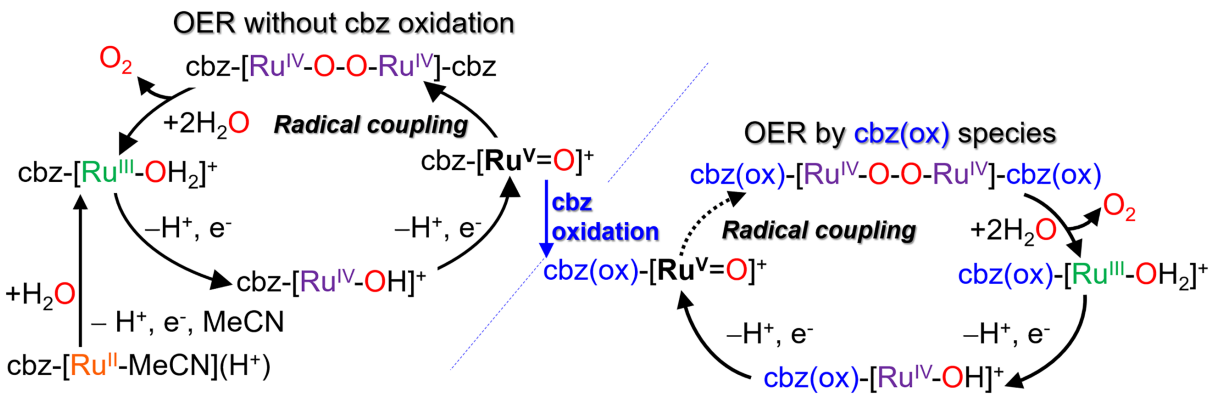

Scheme 1. Possible OER mechanism of **C1** and **C2** involving the oxidation of the cbz moiety.

the TON was approximately 1.6 times higher than that of **C0**. We next examined the photochemical OER of **C0** in the presence of two equivalents of cbz-H to determine the contribution of the cbz moiety (Fig. S13). In contrast to the chemical OER [Fig. 6(a)], the addition of cbz-H hardly affected the photochemical OER of **C0**, suggesting that the oxidation of cbz does not significantly affect the photo-oxygenation reaction. Considering the redox potentials of $[Ru(bpy)_3]$-type PSs (ground state $Ru^{III/II}$, ~1.27 V and ^{3}MLCT excited $Ru^{II*/I}$, ~0.96 V), [16] the Ru centres of **C1** and **C2** can be oxidized by these PS species, while the cbz moiety cannot be oxidized. However, in the photolysis using a $[Ru(bpy)_3]^{2+}$ PS and $Na_2S_2O_8$ sacrificial oxidant, the sulfate radical, generated by the one-electron reduction of the persulfate anion was reported to be a sufficiently strong oxidant (>2.4 V vs NHE [17]) to decompose the $[Ru(bpy)_3]^{2+}$ oxidatively. [18] The UV-vis absorption spectra after 1 h of photochemical OER were obtained to evaluate the stability of the $[Ru(bpy)_3]^{2+}$ photosensitizer (Fig. S14). The ^{1}MLCT absorption band at ~450 nm decreased to almost half in the absence of a catalyst after 1 h of reaction, while the decrease in ^{1}MLCT absorption was effectively suppressed in the order **C0** < **C1** < **C2**. Notably, in the reaction with **C2**, hardly any changes were observed in both the absorbance and width of the ^{1}MLCT band after 1 h of photochemical OER, indicating the negligible decomposition of $[Ru(bpy)_3]^{2+}$ PS. In addition, the absorption peak at 316 nm was assigned to the oxidative decomposed species of the Ru photosensitizer. [18a] Thus, the decreasing photochemical OER activity of **C2** within 10 min of reaction should not be due to the decomposition of the $[Ru(bpy)_3]^{2+}$ PS. Considering that the cbz oxidation wave of **C2** in the CV measurement decreased more rapidly by only a few potential sweeps than that of **C1** (Fig. S4), the decreasing photochemical OER activity of **C2** can be associated with the oxidative decomposition of the cbz moiety by sulfate radicals to form a less active species. This is also supported by the photochemical OER reaction in the presence of one-electron sacrificial oxidant $[Co^{III}Cl(NH_3)_5]^{2+}$ [19];

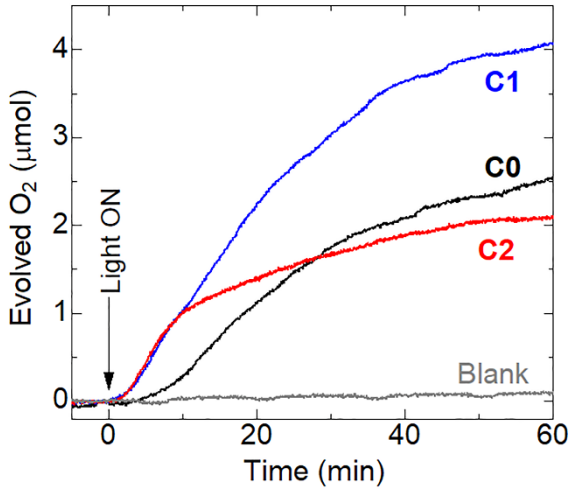

Fig. 7. Photochemical OER plots of the complexes **C0** (black), **C1** (blue), and **C2** (red) in borate buffer (10 mM, pH = 8.0) aq./TFE /acetonitrile (v/v/v = 3/2/1). [Cat.] = 10 μM, $[Ru(bpy)_3]^{2+}$ = 200 μM, $[Na_2S_2O_8]$ = 5 mM, λ = 470 nm, 30 mWcm^{-2}.

Table 3. Photocatalytic O_2 evolution activity of each WOC. [a]

Catalyst	TOF_{max}(min^{-1}) [b]	TON [c]
C0	1.5	49
C1	2.7	79
C2	2.7	40

[a] Borate buffer (10 mM, pH8.0) aq./TFE/acetonitrile (v/v/v = 3/2/1) [Cat.] = 10 μM, $[Ru(bpy)_3]^{2+}$ = 200 μM, $[Na_2S_2O_8]$ = 5 mM, λ = 470 ± 10 nm, 30 mWcm^{-2}. [b] Estimated from the values at 15–20 min (**C0**) and 3–8 min (others) after light irradiation. [c] Estimated from the values at 60 min after light irradiation.

the decrease of photochemical OER rate of **C2** within 10 min irradiation was hardly observed and the evolved O_2 amount of **C2** after 60 min irradiation was comparable to that of **C1** (Fig. S15).

Conclusions

We synthesized the $[Ru(bda)(py)_2]$-type OER molecular catalysts **C1** and **C2**, with one and two carbazole (cbz) group(s), respectively, as precursors of hole-mediators and investigated the effect of cbz functionalization on the photophysical and OER activity as compared to that of the unsubstituted **C0**. Theoretical calculations, spectroscopic and electrochemical measurements revealed the cbz moiety functions as electron-withdrawing groups that improve the OER activity in both chemical OER in the presence of CAN and photochemical OERs comprising a $[Ru(bpy)_3]^{2+}$ photosensitizer and $Na_2S_2O_8$. Even at a low catalyst concentration (25 μM), **C2** completely consumed CAN to generate O_2. In the chemical OER with a large excess of CAN, both **C1** and **C2** exhibited unique behaviour, in which the OER activity changed during the reaction. This indicated competition between the oxidation of the cbz moiety and OER at the Ru centre. In the photochemical OER, both **C1** and **C2** exhibited high initial OER activities. A rapid deactivation behaviour was observed for **C2**, while **C1** showed higher OER activity and durability comparable to that of the unsubstituted **C0**. This suggested that the number of cbz groups in the catalyst molecule is key to this behaviour. The preparation of photoelectrodes based on these molecular catalysts is currently in progress.

Experimental

Synthesis and Materials

2, 2'-Bipyridyl-6, 6'-dicarboxylic acid ($bdaH_2$), [20a] 9-(pyridyn-4-yl)-9H-carbazole (cbz-py), [20b] $[Ru(bda)(pyridine)_2]$ (**C0**), [10a,b] $[RuCl_2(DMSO)_4]$, [20c] $[Ru(bda)(DMSO)_2]$, [20d] $[Ru(bda)(4\text{-bromopyridine})_2]$ (**C0-Br**), [10a] and $[Ru(bpy)_3](SO_4)$ [20e] were synthesized according to previously reported methods. **C0**, **C0-Br**, **C1**, and **C2** were stored in a nitrogen-filled glovebox [10a, 11, 13] until use. High-purity water was obtained by passing house-distilled water through a Millipore Milli-Q Simplicity® UV system. All other reagents and solvents were purchased from commercial sources and used as received.

Synthesis of [Ru(bda)(cbz-py)(pyridine)] (C1).

[Ru(bda)(DMSO)$_2$] (203.8 mg, 0.41 mmol, 1 eq.), pyridine (33 μL, 0.40 mmol, 1 eq.), and methanol (10 mL) were added to a two-necked round-bottom flask and bubbled with N_2 for 10 min. The resultant dark-red solution was stirred at 313 K under N_2 for 5 min, after which cbz-py (101.2 mg, 0.41 mmol, 1 eq.) was added under N_2 flow. The reaction mixture was then refluxed under N_2 for 4 h. After cooling to 293 K, the solvent was removed using a rotary evaporator, and the obtained dark-red crude powder was subjected to silica-gel column chromatography. (Eluent: CH_2Cl_2/methanol = 10/1). The second red band (R_f = 0.16) was collected, and the solvent removed. Finally, the product was recrystallized by the gas–liquid diffusion method with CH_2Cl_2/methanol-diethyl ether and dried in vacuo to afford dark-red needle-like crystals. Yield: 106.1 mg (0.16 mmol, 39%). ^{1}H NMR (Fig. S16a, 400 MHz, CD_2Cl_2/methanol-d_4 with a small amount of L-ascorbic acid): δ = 8.46 (d, *J* = 8.0 Hz, 2H), 8.13–8.08 (m, 4H), 8.03 (d, J = 6.6 Hz, 2H), 7.92–7.86 (m, 4H), 7.84 (t, *J* = 7.8 Hz, 1H), 7.54–7.50 (m, 4H), 7.40 (td, 2H, *J* = 1.4, 7.3 Hz), 7.32 (2H, t, *J* = 7.7 Hz), 7.18 (2H, t, *J* = 1.4, 7.2 Hz). MALDI-TOF MS (positive mode, CH_2Cl_2/methanol) *m/z*$^+$ = 667.08. (**C1**+H$^+$) calcd. 667.65. Elemental analysis calcd. for $C_{34.4}Cl_{0.8}H_{23.8}N_5O_4Ru$ ([**C1**]·0.4CH_2Cl_2): C, 58.97; H, 3.42; N, 10.00. Found: C, 59.09; H, 3.39; N, 9.85.

Synthesis of [Ru(bda)(cbz-py)$_2$] (C2).

[Ru(bda)(DMSO)$_2$] (102.7 mg, 0.21 mmol, 1 eq.), cbz-py (100.1 mg, 0.41 mmol, 2 eq.) and methanol (10 mL) were added to a two-necked round-bottom flask and bubbled with N_2 for 15 min. The resultant dark-red solution was refluxed under N_2 for 8 h. After cooling to 293 K, the reaction mixture was filtered and washed with acetone several times until the filtrate became colourless. The obtained dark-red powder was dried in air and then extracted twice with chloroform/L-ascorbic acid aqueous solution. Subsequently, the organic phase was washed with water and dried with Na_2SO_4, and the solvent was evaporated. The resulting dark-red powder was recrystallized by the gas–liquid diffusion method with diethyl ether-CH_2Cl_2/methanol and dried in vacuo to afford dark-red needle-like crystals. Yield: 78.0 mg (0.080 mmol, 38%). ^{1}H NMR (Fig. S16b, 400 MHz, CD_2Cl_2/methanol-d_4 with a small amount of L-ascorbic acid): δ = 8.38 (d, *J* = 7.8 Hz, 2H), 8.17 (dd, *J* = 0.9, 7.8 Hz 2H), 8.09 (d, *J* = 7.8 Hz, 4H), 8.01 (dd, *J* = 1.4, 5.5 Hz, 4H), 7.87 (t, *J* = 7.8 Hz, 2H), 7.52 (d, 4H, *J* = 8.2 Hz), 7.49 (4H, dd, *J* = 1.4, 5.5 Hz), 7.41 (4H, td, *J* = 1.4, 7.8 Hz), 7.32 (4H, td, *J* = 0.9, 7.8 Hz). MALDI-TOF MS (positive mode, CH_2Cl_2/methanol) *m/z*$^+$ = 832.13. (**C2**+H$^+$) calcd. 832.84. Elemental analysis. calcd. for $C_{46.5}ClH_{31}N_6O_4Ru$ ([**C2**]·0.5CH_2Cl_2): C, 63.88; H, 3.57; N, 9.61. Found: C, 63.88; H, 3.51; N, 9.61. Single crystals of **C2** were obtained by the gas-liquid diffusion method with diethyl ether-CH_2Cl_2/methanol.

Measurements

^{1}H NMR spectra were recorded using a JEOL ECZ-400S instrument. Elemental analysis was conducted at the analysis centre of Hokkaido University. MALDI-TOFMS measurements were carried out using a Bruker Autoflex Speed instrument, with α-cyano-4-hydroxycinnamic acid as the matrix. IR spectra were recorded on a JASCO FT-IR 4100 spectrophotometer using KBr pellets. Single-crystal X-ray diffraction data were collected using a Rigaku XtaLAB Synergy diffractometer equipped with Cu Kα radiation (PhotonJet (Cu)). Each crystal was mounted on a MicroMount using paraffin oil. The crystal was then cooled using a N_2-flow-type temperature controller. The diffraction data were processed using CrysAlisPRO software. [21] The structures were solved by direct methods using SHELXT [22] and refined by full-matrix least-squares refinement using SHELXL. [23] Non-hydrogen atoms were refined anisotropically, while the hydrogen atoms were refined using the riding model. All calculations were performed using the Olex2 software package. [24] The crystallographic data obtained for **C2** are listed in Table S2. † Full crystallographic data have been deposited with the Cambridge Crystallographic Data Centre (CCDC 2103846).† UV–vis absorption spectra were recorded on Shimadzu UV-2400PC or Hitachi U-3000 spectrophotometers. Electrochemical measurements (CV and DPV) were recorded using a HOKUTO DENKO HZ-3000 electrochemical measurement system equipped with glassy carbon, Pt wire, and Ag/AgCl (aqueous mixture) or Ag/Ag$^+$ (organic solvents) electrodes as the working, counter, and reference electrodes, respectively. Solutions of aqueous solution (pH = 1.0–8.0, pH adjusted by $HClO_4$/40 mM of Britton-Robinson buffer/NaOH)/2,2,2-trifluoroethanol(TFE) /acetonitrile (v/v/v = 1/2/1 for CV or 3/2/1 for the other measurements) containing 0.1 M sodium perchlorate ($NaClO_4$) or dichloromethane/TFE (v/v = 9/1) containing 0.1 M tetrabutylammonium hexafluorophosphate ($TBAPF_6$) as the supporting electrolyte were used in the electrochemical measurements. All solutions were deaerated by N_2 bubbling for 15 min before measurement.

Chemical Water Oxidation

A solution of $(NH_4)_2[Ce(NO_3)_6]$ (CAN, 240 mM) in $HClO_4$ aqueous solution (2.5 mL, pH = 1.0) was placed in a glass vessel (volume ~87.8 mL) with vigorous stirring (296 ± 1 K). A solution of the ruthenium catalyst (0–200 μM) in TFE/acetonitrile (v/v = 2/1, 2.5 mL) was injected into the CAN solution; these solutions were deaerated by Ar bubbling for ~30 min before injection. The amount of evolved oxygen was monitored using a FireSting oxygen monitor (PyroScience GmbH). The OER rate and TOF were estimated using the following formulae from the amount of evolved O_2:

OER rate (mMs^{-1}) = evolved O_2 (μmol) / 5 mL × time (s)

TOF (s^{-1}) = 1000 × OER rate / [Cat.] (μM)

Photochemical Water Oxidation

In the dark, aqueous borate buffer/TFE/acetonitrile (v/v/v = 3/2/1) solution (10 mM, pH = 8.0 [10d, 25]) containing [Ru(bpy)$_3$](SO$_4$) photosensitizer (200 μM), water oxidation catalyst (10 μM), and $Na_2S_2O_8$ (5 mM) was placed in a Pyrex vial (volume ~21.2 mL) with a small magnetic stirring bar and covered with a rubber septum. The resultant solution (total 5 mL) was deoxygenated by bubbling with Ar gas for 30 min. The amount of evolved oxygen was monitored using a FireSting oxygen monitor (PyroScience GmbH). The vials were irradiated with a blue LED lamp (λ = 470 ± 10 nm; 30 mW; OptoDevice Lab. Ltd., OP6-4710HP2). The temperature was controlled at 296 ± 1 K using an in-house aluminium water-cooling jacket with a water-circulating temperature controller (EYELA CCA-1111).

Theoretical calculation

Calculations were performed using the Gaussian 09 software package.[26] For **C2**, the molecular structure was determined by X-ray structure analysis, and the obtained structure was used as the initial structure for the calculation. (Fig. S17 and Table S5) Geometry optimizations and TD-DFT calculation were performed in the ground state using the B3LYP functional[27] together with the 6-31G basis set[28] on C, H, N, and O atoms. The LANL2DZ effective core potentials and associated basis set were used on the Ru atom.[29] Although the results of **C0** calculated under the same basis/functional set with Gaussian 03 have already been reported, [10d] we carried out re-calculations using Gaussian 09 for a more precise comparison with the values of **C1** and **C2**. The difference in the frontier orbital energy values was negligible (<0.001 eV).

Author Contributions

Conceptualisation, A.K.; investigation, H.O.; resources, A.K. and M.K.; methodology, A.K. and H.O.; formal analysis and data curation H.O., M.Y., and A.K.; writing—original draft preparation, H.O.; writing—review and editing, A.K.; visualisation, A.K.; supervision, M.K.; project administration, A.K.; funding acquisition, A.K. and M.K.

Conflicts of interest

There are no conflicts to declare.

Acknowledgements

This study was supported by the ENEOS Hydrogen Trust Fund and JSPS KAKENHI (Grant Numbers JP18K19086, JP17H06367, and JP20H05082).

References

1 H. Inoue, T. Shimada, Y. Kou, Y. Nabetani, D. Masui, S. Takagi and H. Tachibana, *ChemSusChem.*, 2011, **4**, 173.
2 (*a*) M. D. Kärkäs, E. V. Johnston, O. Verho and B. Åkermark, *Acc. Chem. Res.*, 2014, **47**, 100. (*b*) M. D. Kärkäs, O. Verho, E. V. Johnston and B. Åkermark, *Chem. Rev.*, 2014, **114**, 11863. (*c*) J. D. Blakemore, R. H. Crabtree and G. W. Brudvig, *Chem. Rev.*, 2015, **115**, 12974. (*d*) R. Matheu, P. Garrido-Barros, M. Gil-Sepulcre, M. Z. Ertem, X. Sala, C. Gimbert-Suriñach and A. Llobet, *Nat. Rev. Chem.*, 2019, **3**, 331. (*e*) M. Kondo, H. Tatewaki and S. Masaoka, *Chem. Soc. Rev.*, 2021, **50**, 6790.
3 (*a*) D. L. Ashford, M. K. Gish, A. K. Vannucci, M. K. Brennaman, J. L. Templeton, J. M. Papanikolas and T. J. Meyer, *Chem. Rev.* 2015, **115**, 13006. (*b*) F. Li, Y. Jiang, B. Zhang, F. Huang and Y. Gao, L. Sun, *Angew. Chem. Int. Ed.*, 2012, **51**, 2417. (*c*) L. Wang, M. Mirmohades, A. Brown, L. Duan, F. Li, Q. Daniel, R. Lomoth, L. Sun and L. Hammarström, *Inorg. Chem.*, 2015, **54**, 2742.
4 (*a*) M. K. Brennaman, R. J. Dillon, L. Alibabaei, M. K. Gish, C. J. Dares, D. L. Ashford, R. L. House, G. J. Meyer, J. M. Papanikolas and T. J. Meyer, *J. Am. Chem. Soc.*, 2016, **138**, 13085. (*b*) J. J. Concepcion, J. W. Jurss, P. G. Hoertz and T. J. Meyer, *Angew. Chem. Int. Ed.* 2009, **48**, 9473. (*c*) B. D. Sherman, Y. Xie, M. V. Sheridan, D. Wang, D. W. Shaffer, T. J. Meyer and J. J. Concepcion, *ACS Energy Lett.*, 2017, **2**, 124. (*d*) M. Yamamoto, L. Wang, F. Li, T. Fukushima, K. Tanaka, L. Sun and H. Imahori, *Chem. Sci.*, 2016, **7**, 1430. (*e*) D. Antón-García, J. Warnan and E. Reisner, *Chem. Sci.*, 2020, **11**, 12769.
5 (*a*) D. Wang, R. N. Sampaio, L. Troian-Gautier, S. L. Marquard, B. H. Farnum, B. D. Sherman, M. V. Sheridan, C. J. Dares, G. J. Meyer and T. J. Meyer, *J. Am. Chem. Soc.*, 2019, **141**, 7926. (*b*) D. Wang, F. Niu, M. J. Mortelliti, M. V. Sheridan, B. D. Sherman, Y. Zhu, J. R. McBride, J. L. Dempsey, S. Shen, C. J. Dares, F. Li and T. J. Meyer, *Proc. Natl. Acad. Sci.*, 2020, **117**, 12564.
6 (*a*) K. Karon and M. Lapkowski, *J. Solid State Electrochem.*, 2015, **19**, 2601. (*b*) L. Kortekaas, F. Lancia, J. D. Steen and W. R. Browne, *J. Phys. Chem. C*, 2017, **121**, 14688. (*c*) M. Li, *Chem. - A Eur. J.*, 2019, **25**, 1142.
7 Z. Singh, P. R. Donnarumma and M. B. Majewski, *Inorg. Chem.*, 2020, **59**, 12994.
8 (*a*) H. Iwami, M. Okamura, M. Kondo and S. Masaoka, *Angew. Chem. Int. Ed.*, 2021, **60**, 5965. (*b*) J. Zhang, J. Du, J. Wang, Y. Wang, C. Wei and M. Li, *Angew. Chem. Int. Ed.*, 2018, **57**, 16698.
9 (*a*) B. Zhang and L. Sun, *J. Am. Chem. Soc.* 2019, **141**, 5565. (*b*) L. Duan, A. Fischer, Y. Xu and L. Sun, *J. Am. Chem. Soc.* 2009, **131**, 10397. (*c*) L. Duan, F. Bozoglian, S. Mandal, B. Stewart, T. Privalov, A. Llobet and L. Sun, *Nat. Chem.*, 2012, **4**, 418.
10 (*a*) Y. Xie, D. W. Shaffer and J. J. Concepcion, *Inorg. Chem.*, 2018, **57**, 10533. (*b*) B. J. J. Timmer, O. Kravchenko, T. Liu, B. Zhang and L. Sun, *Angew. Chem.*, 2021, **133**, 14625. (*c*) L. Duan, L. Wang, A. K. Inge, A. Fischer, X. Zou and L. Sun, *Inorg. Chem.*, 2013, **52**, 7844. (*d*) Y. Sato, S. Takizawa and S. Murata, *Eur. J. Inorg. Chem.*, 2015, 5495.
11 N. Song, J. J. Concepcion, R. A. Binstead, J. A. Rudd, A. K. Vannucci, C. J. Dares, M. K. Coggins and T. J. Meyer, *Proc. Natl. Acad. Sci.*, 2015, **112**, 4935.
12 E. T. Veiga, A. V. Müller, L. D. Ramos, K. P. M. Frin and A. S. Polo, *Eur. J. Inorg. Chem.*, 2018, 2680.
13 D. W. Shaffer, Y. Xie, D. J. Szalda and J. J. Concepcion, *Inorg. Chem.*, 2016, **55**, 12024.
14 E. Wadsworth, F. R. Duke and C. A. Goetz, *Anal. Chem.*, 1957, **29**,1824.
15 (*a*) M. A. Ponce and R. Erra-Balsellsnitro, *J. Heterocycl. Chem.*, 2001, **38**, 1071. (*b*) M. Chakrabarty and A. Batabyal, *Synth. Commun.*, 1994, **24**, 1
16 C. R. Bock, J. A. Connor, A. R. Gutierrez, T. J. Meyer, D. G. Whitten, B. P. Sullivan and J. K. Nagle, *J. Am. Chem. Soc.*, 1979, **101**, 4815.
17 D. M. Stanbury, *Adv. Inorg. Chem.*, 1989, **33**, 69.
18 (*a*) U. S. Akhtar, E. L. Tae, Y. S. Chun, I. C. Hwang and K. B. Yoon, *ACS Catal.*, 2016, **6**, 8361. (*b*) B. Limburg, E. Bouwman and S. Bonnet, *ACS Catal.*, 2016, **6**, 5273.
19 N. Curtis, G. Lawrance, A. Sargeson, *Aust. J. Chem.* 1983, **36**, 1327.
20 (*a*) C. L. Donnici, D. H. M. Filho, L. L. C. Moreira, G. T. dos Reis, E. S. Cordeiro, I. M. F. de Oliveira, S. Carvalho and E. B. Paniago, *J. Braz. Chem. Soc.*, 1998, **9**, 455. (*b*) T. Morofuji, H. Kinoshita and N. Kano, *Chem. Commun.*, 2019, **55**, 8575. (*c*) E. Dulière, M. Devillers and J. Marchand-Brynaert, *Organometallics,* 2003, **22**, 804. (*d*) L. Wang, K. Fan, Q. Daniel, L. Duan, F. Li, B. Philippe, H. Rensmo, H. Chen, J. Sun and L. Sun, *Chem. Commun.*, 2015, **51**, 7883. (*e*) D. Hong, S. Mandal, Y. Yamada, Y. M. Lee, W. Nam, A. Llobet and S. Fukuzumi, *Inorg. Chem.*, 2013, **52**, 9522.
21 *CrysAlisPro*, version 1.171.39.45h, Rigaku Corporation, Oxford, UK, 2018.

22 G. M. Sheldrick, *Acta Crystallogr., Sect. A: Found. Adv.*, 2015, **71**, 3.
23 G. M. Sheldrick, *Acta Crystallogr., Sect. C: Struct. Chem.*, 2015, **71**, 3.
24 O. V. Dolomanov, L. J. Bourhis, R. J. Gildea, J. A. K. Howard and H. Pushmann, Olex2, *J. Appl. Crystallogr.*, 2009, **42**, 339.
25 S. Berardi, G. La Ganga, M. Natali, I. Bazzan, F. Puntoriero, A. Sartorel, F. Scandola, S. Campagna and M. Bonchio, *J. Am. Chem. Soc.*, 2012, **134**, 11104.
26 *Gaussian 09, Revision E.01*, M. J. Frisch, G. W. Trucks, H. B. Schlegel, G. E. Scuseria, M. A. Robb, J. R. Cheeseman, G. Scalmani, V. Barone, B. Mennucci, G. A. Petersson, H. Nakatsuji, M. Caricato, X. Li, H. P. Hratchian, A. F. Izmaylov,j. Bloino, G. Zheng, J. L. Sonnenberg, M. Hada, M. Ehara, K. Toyota, R. Fukuda, J. Hasegawa, M. Ishida, T. Nakajima, Y. Honda, O. Kitao, H. Nakai, T. Vreven, J. A. Montgomery, Jr., J. E. Peralta, F. Ogliaro, M. Bearpark, J. J. Heyd, E. Brothers, K. N. Kudin, V. N. Staroverov, R. Kobayashi, J. Normand, K. Raghavachari, A. Rendell, J. C. Burant, S. S. Iyengar, J. Tomasi, M. Cossi, N. Rega, J. M. Millam, M. Klene, J. E. Knox, J. B. Cross, V. Bakken, C. Adamo, J. Jaramillo, R. Gomperts, R. E. Stratmann, O. Yazyev, A. J. Austin, R. Cammi, C. Pomelli, J. W. Ochterski, R. L. Martin, K. Morokuma, V. G. Zakrzewski, G. A. Voth, P. Salvador, J. J. Dannenberg, S. Dapprich, A. D. Daniels, Ö. Farkas, J. B. Foresman, J. V. Ortiz, J. Cioslowski, D. J. Fox, Gaussian, Inc., Wallingford CT, 2009.
27 (a) A. D. Becke, *J. Chem. Phys*., 1993, **98**, 5648. (b) C. Lee, W. Yang, R. G. Parr, *Phys. Rev. B*, 1988, **37**, 785.
28 (a) D. Andrae, U. Haussermann, M. Dolg, H. Stoll, H. Preuss, *Theor. Chem. Acta*., 1990, **77**, 123. (b) W. Küechle, M. Dolg,H. Stoll, H. Preuss, *J. Chem. Phys*., 1994, **100**, 7535.
29 (a) P. J. Hay,W. R. Wadt, *J. Chem. Phys*. 1985, **82**, 270. (b) W. R. Wadt, P. J. Hay, *J. Chem. Phys*. 1985, **82**, 284. (c) P. J. Hay,W. R. Wadt, *J. Chem. Phys*. 1985, **82**, 299.